CHAPTER 5

TRIBOLOGICAL BEHAVIOUR OF GRAPHENE AS AN ADDITIVE IN WATER

The current chapter describes the results on the characterisation of the stainless steel, graphene oxide powder and its dispersion in water. The results on the friction and wear characteristics of steel against steel tribo-pair under reciprocating sliding and lubricated with dispersed graphene oxide in water are also included in the chapter. The results have also been discussed to develop a coherent understanding of the role of graphene oxide as an additive in water in controlling the friction and wear between the tribo-pair.

5.1 RESULTS

5.1.1 CHEMICAL COMPOSITION OF STAINLESS STEEL

The chemical composition of the stainless steel, as analysed through energy-dispersive X-ray spectroscopy, has been given in Table 5.1.

Table 5.1 Chemical composition of stainless steel (wt. %).

C	O	Fe	Cr	Ni	Mn	Si
0.08	1.73	68.83	18.23	8.94	1.76	0.43

5.1.2 SURFACE ROUGHNESS OF STAINLESS STEEL

Figure 5.1 shows the topography of the polished stainless steel specimen, as examined by a non-contact 3D profilometer. It can be observed that the root mean square surface roughness is lower than 20 nm.

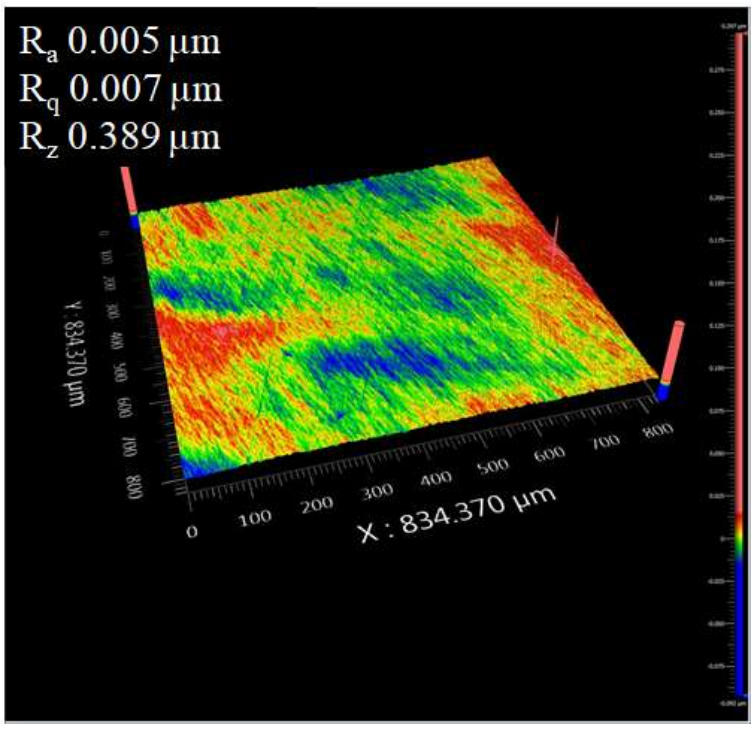

Fig. 5.1 Surface roughness of stainless steel measured by a 3D optical profilometer.

5.1.3 CHARACTERISATION OF GRAPHENE OXIDE POWDER

Figure 5.2 represents the Raman spectrum of graphene oxide powder, which shows the presence of a D peak at 1349 cm^{-1}, a G peak at 1589 cm^{-1}, and a weak intensity 2D peak at 2715 cm^{-1}. Another weak intensity peak D+D′ can also be observed at 2932 cm^{-1}.

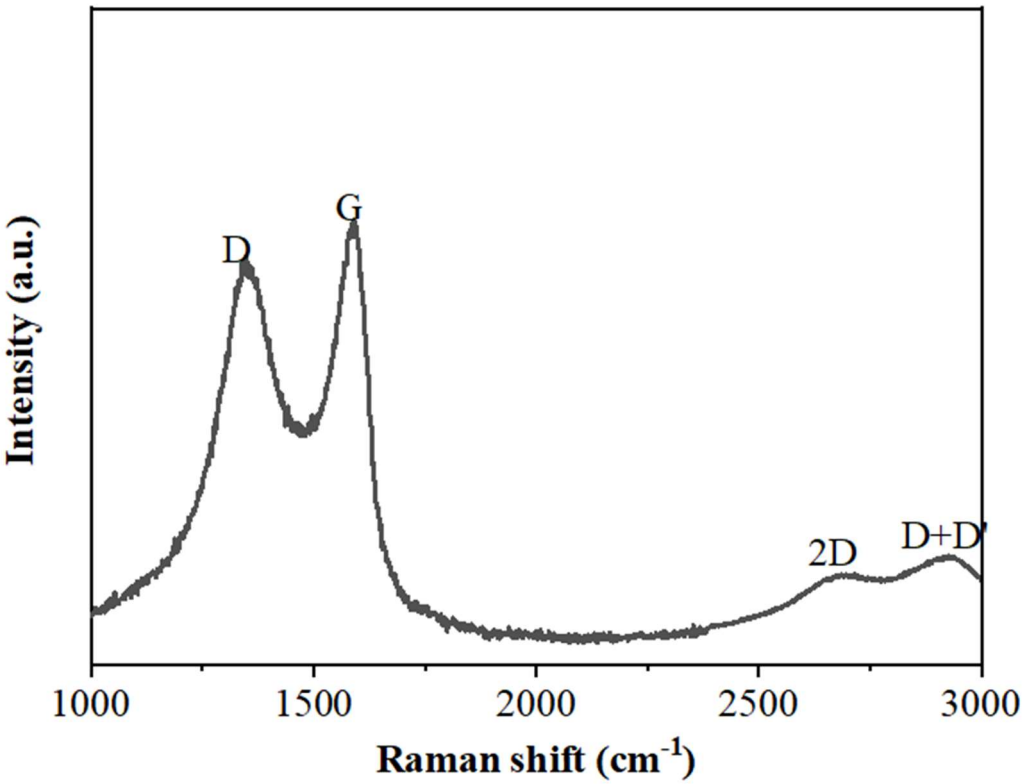

Fig. 5.2 Raman spectrum of graphene oxide powder.

5.1.4 CHARACTERISTICS OF DISPERSED GRAPHENE OXIDE

Figure 5.3 illustrates the digital images of graphene oxide-water dispersion after 2 h sonication with different concentrations (0.01, 0.05, 0.1, and 0.5 wt. %) of graphene oxide. Atomic force microscope (AFM) and transmission electron microscope (TEM) have been used to characterise the dimensions of graphene oxide nano-sheets dispersed in water. Figure 5.4 shows a 2D AFM image and corresponding height profile (at a particular section lined in the 2D image) of some dispersed nano-sheets. The thickness of the sheets is observed to be ~ 1.2 nm. However, a higher thickness of ~ 2.4 nm can be seen at the centre in the AFM image. Figure 5.5 presents a TEM image of dispersed graphene oxide nano-sheets, and one may observe that the size of sheets is lower than 5 μm.

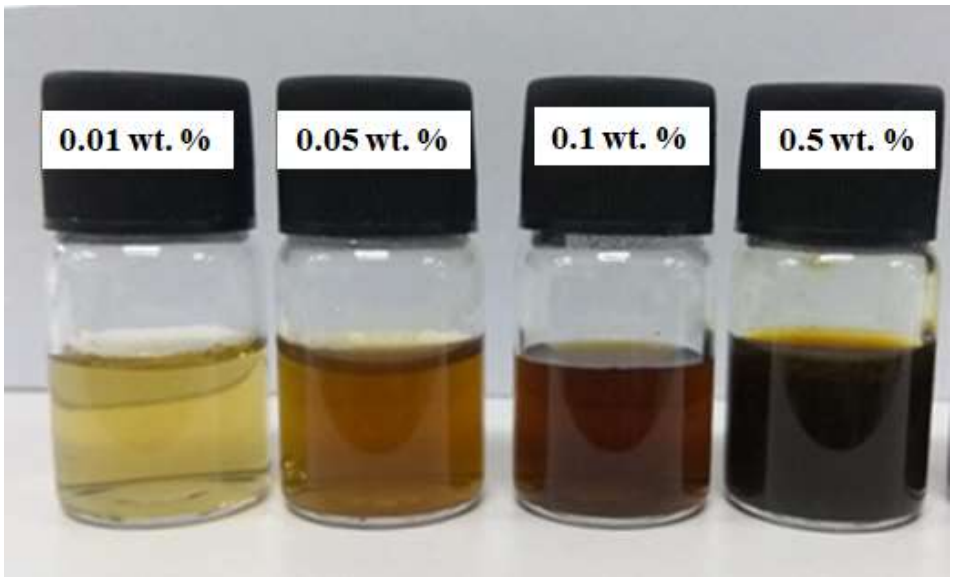

Fig. 5.3 Digital images of graphene oxide-water dispersion after 2 h sonication with different concentrations of graphene oxide.

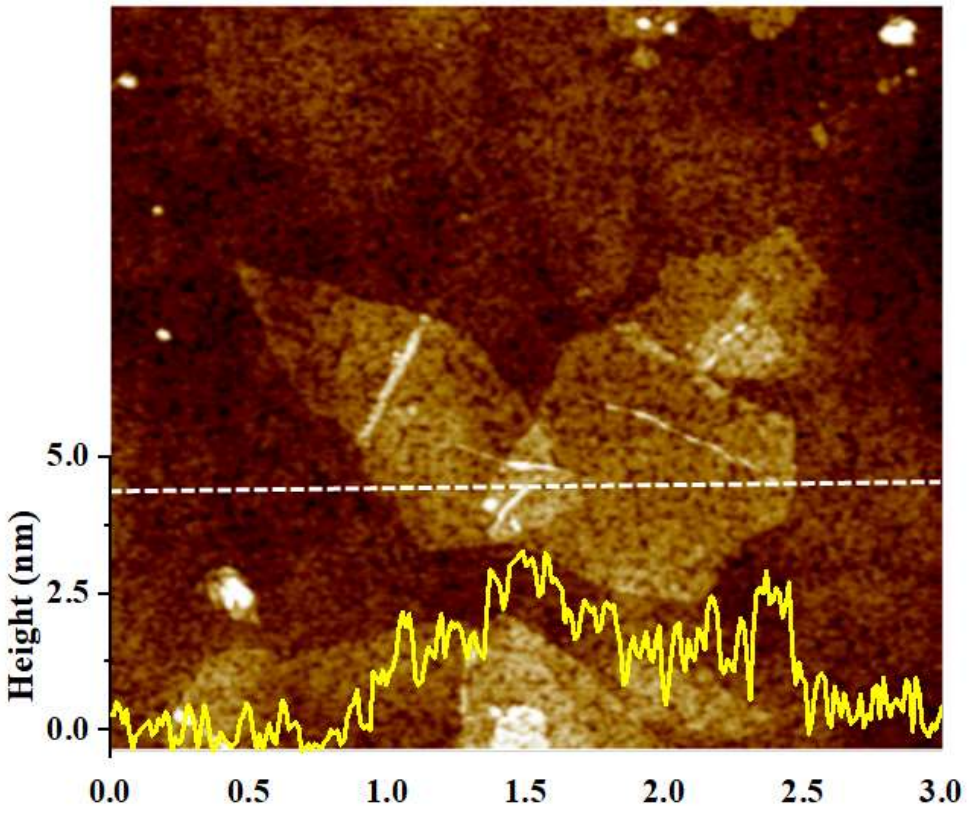

Fig. 5.4 2D AFM image and height profile across the line of dispersed graphene oxide.

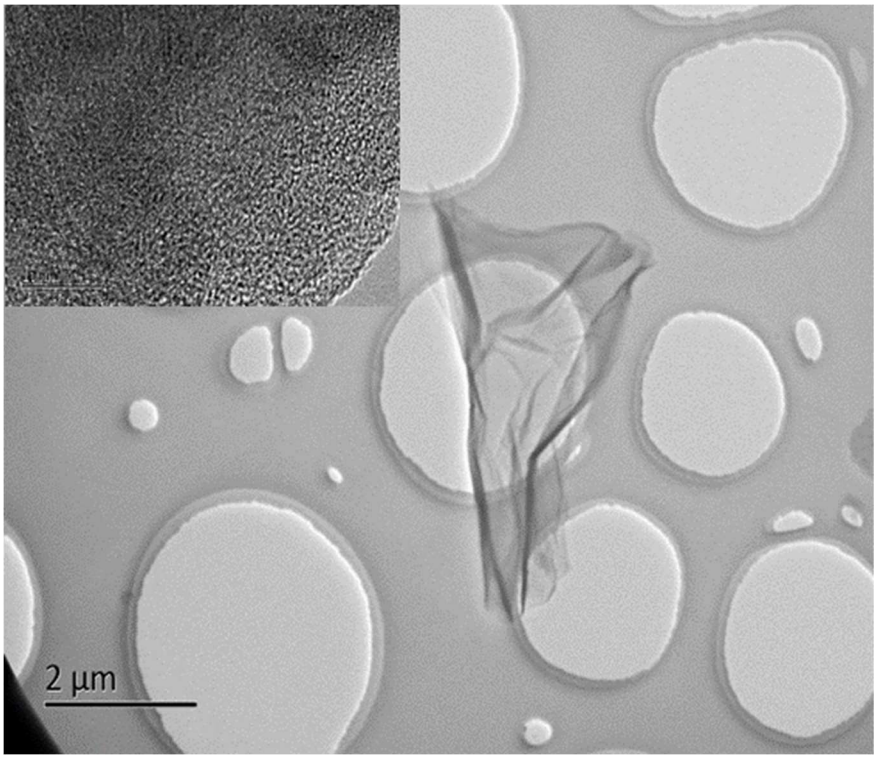

Fig. 5.5 TEM image of the dispersed graphene oxide powder.

5.1.5 RHEOLOGICAL PROPERTIES OF GRAPHENE OXIDE-WATER DISPERSIONS

The rheological properties play a significant role in lubrication. Therefore, the rheological behaviour of the dispersions, having different concentrations of graphene oxide in water, has been determined by using a rheometer with cone-plate geometry. Figure 5.6 illustrates the variation of dynamic viscosity with shear rate, and one may infer that the viscosity of water-graphene oxide dispersion increases with an increasing amount of graphene oxide in water.

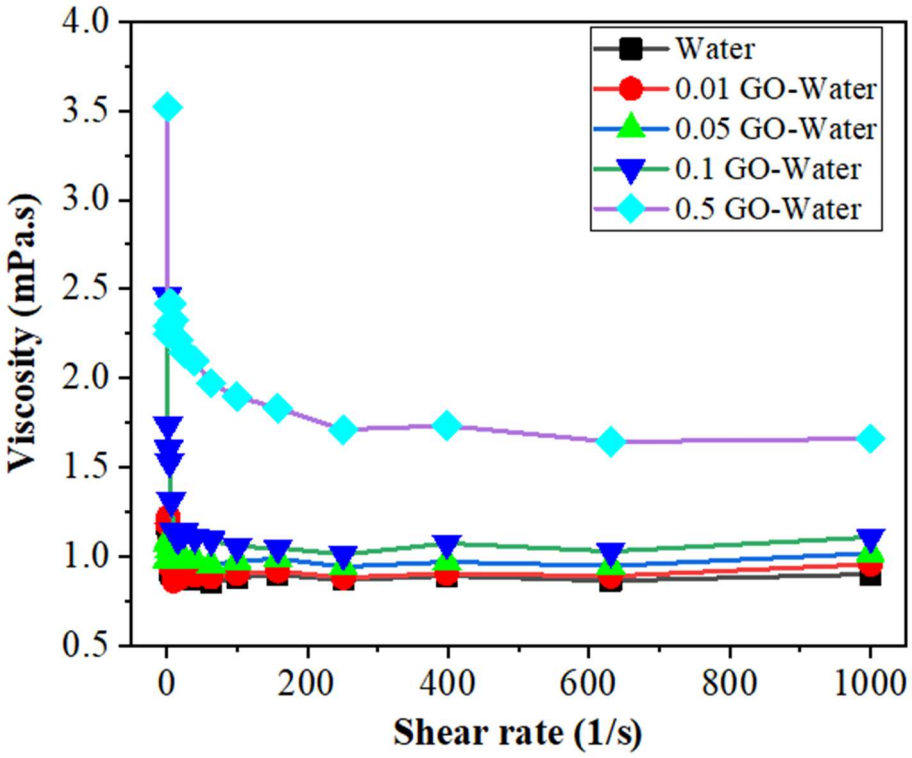

Fig. 5.6 Variation of the dynamic viscosity as a function of shear rate for different concentrations of graphene oxide in water.

5.1.6 RECIPROCATING FRICTION AND WEAR BEHAVIOUR

5.1.6.1 Effect of Concentration on Tribological Behaviour

5.1.6.1.1 Friction behaviour

It is well known that the concentration of lubricant plays a vital role in enhancing the anti-friction and anti-wear characteristics. Friction and wear tests under reciprocating motion have been conducted to investigate the effect of the varying concentration of graphene oxide in pure water on the macro-scale tribological performance of self-mated stainless steel tribo-pair at a normal load of 5 N and sliding speed of 0.01 m/s in ambient condition for 3600 cycles. The pure water as a lubricant has

been chosen as a reference for comparing the lubrication capabilities of different concentrations of graphene oxide in water. Figure 5.7 shows the variation of the coefficient of friction with the number of cycles for pure water and for different concentrations of graphene oxide in water at a load of 5 N. It is clear from Fig. 5.7 that the pure water has significant fluctuation and a high coefficient of friction throughout the friction test. The coefficient of friction of the system using pure water is approximately 0.56. However, one could observe that even a small concentration (0.01 wt. %) of graphene oxide in water can significantly reduce the coefficient of friction (COF) of the system, as evident from Fig. 5.7. The addition of 0.1 wt. % of graphene oxide in water has been observed to exhibit a comparatively consistent, and low coefficient of friction throughout the test in comparison to other concentrations as well as pure water.

The variation of the average steady-state coefficient of friction of the system with varying concentrations of graphene oxide in water is presented in Fig. 5.8. A significant reduction in the coefficient of friction is found to occur with the addition of even 0.01 wt. % graphene oxide in pure water, as evident from Fig. 5.8. The average coefficient of friction has been found to decrease with the increasing amount of graphene oxide from 0.01 to 0.1 wt. % followed by a slight increase for 0.5 wt. %, indicating that 0.1 wt. % is the optimum content of graphene oxide in water under the conditions used in the present investigation. The average coefficient of friction for different concentrations of graphene oxide in water, i.e., 0.01, 0.05, 0.1, and 0.5 wt. % have been observed to be 0.38, 0.21, 0.12, and 0.15 respectively. The lower and the higher concentration of graphene oxide have shown relatively higher coefficients of friction in comparison to 0.1 wt. %, as evident from Fig. 5.8. When compared with pure water lubrication, the lubrication with 0.1 wt. % graphene oxide in water has been found to reduce the coefficient of friction of the system by 78% (i.e., from 0.56 to 0.12).

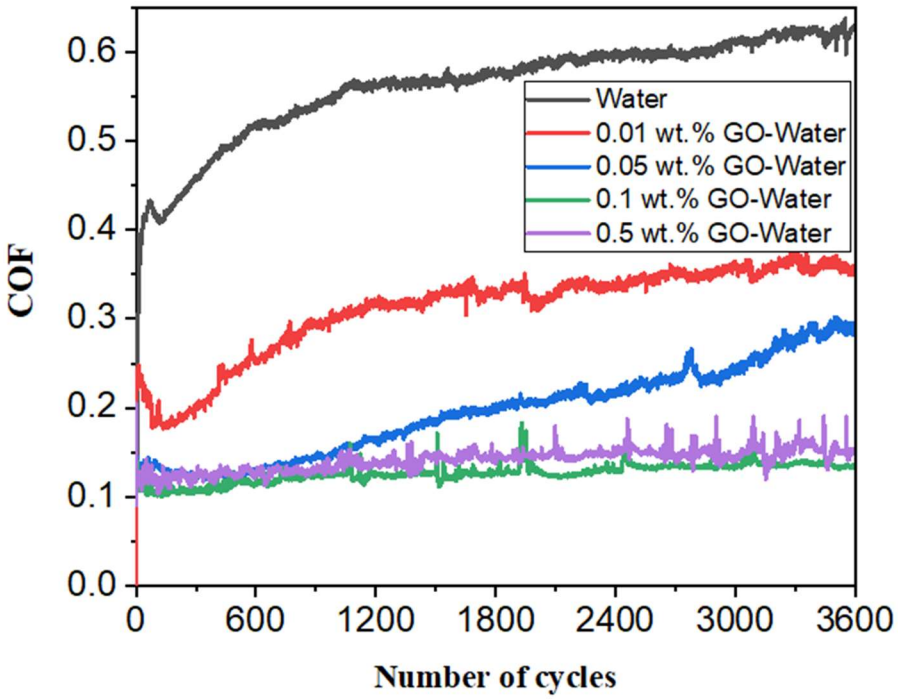

Fig. 5.7 Coefficient of friction as a function of the number of cycles for different concentrations of graphene oxide in water and for pure water at a normal load of 5 N.

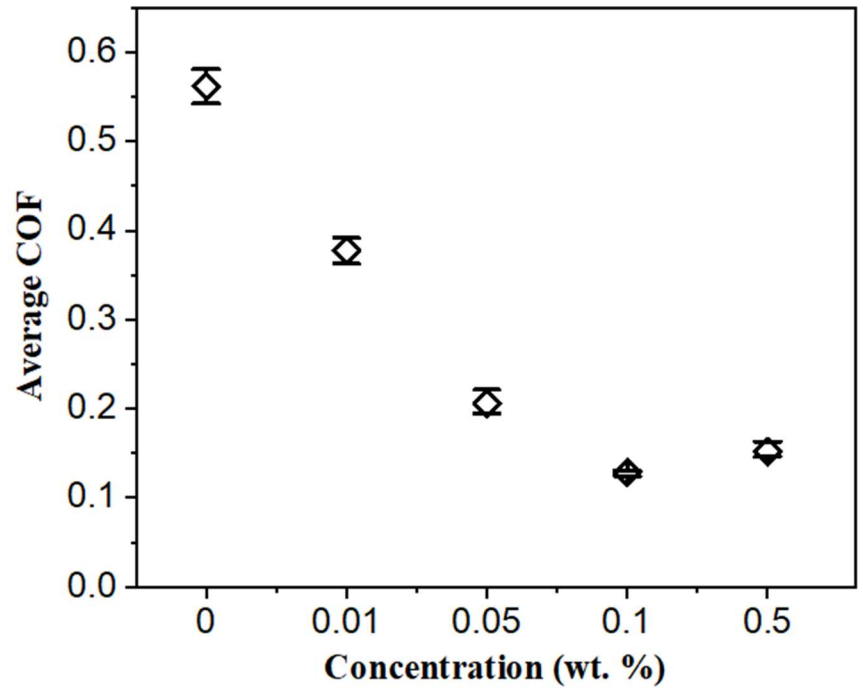

Fig. 5.8 Variation of average coefficients of friction as a function of the concentration of graphene oxide in water at a normal load of 5 N.

5.1.6.1.2 Wear behaviour

The effect of graphene oxide concentration on the wear behaviour of self-mated stainless steel tribo-pair, i.e., ball and disc at a load of 5 N and sliding speed of 0.01 m/s has been examined by conducting reciprocating wear tests. Wear scar diameter on the ball and wear track width on the disc have been considered as the critical parameters for evaluating the anti-wear performance of the lubricants. Figures 5.9 to 5.13 show the optical micrographs of wear scar on the ball and corresponding wear track on discs, respectively, for pure water, 0.01 wt. %, 0.05 wt. %, 0.1 wt. % and 0.5 wt. % of graphene oxide in water after the friction test at a normal load of 5 N and sliding speed 0.01 m/s for 3600 cycles. Under the lubrication with pure water, the severe wear of steel ball, as well as disc, has been observed to occur, which could be seen from Figs. 5.9 (a and b). Figures 5.9 (a and b) depict the wear scar on the ball and wear track on the disc lubricated with pure water as a lubricant, respectively. The wear scar diameter and wear track width for pure water lubrication have been found to be ~ 267 μm and ~ 282 μm, respectively. Further, one could observe a significant reduction in both the wear scar diameter on the ball and the wear track width on the corresponding disc with the addition of 0.01 wt. % graphene oxide in contrast to that observed for pure water lubrication, as evident from a comparison of Figs. 5.10 (a and b) and 5.9 (a and b). The wear scar diameter and wear track width are found to be ~ 204 μm and ~ 219 μm, respectively, for 0.01 wt. % graphene oxide addition. Figure 5.11 shows that the wear scar diameter and wear track width for 0.05 wt. % graphene oxide in water are ~ 183 μm and ~ 191 μm, respectively, whereas the same are found to be ~ 175 μm and ~ 179 μm, respectively, for 0.1 wt. % concentration of graphene oxide in water (Fig. 5.12) indicating thus, a decrease with increasing concentration to 0.1 wt. %. However, both the wear scar diameter and

wear track width are found to increase to ~ 235 µm and ~ 266 µm, respectively, as the concentration of graphene oxide is increased to 0.5 wt. % (Fig. 5.13).

A comparison of wear scars shown in Figs. 5.9 (a), 5.10 (a), 5.11 (a), 5.12 (a), and 5.13 (a) indicates that wear scar diameters reduce with an increasing amount of addition of graphene oxide till 0.1 wt. % and increases thereafter for 0.5 wt. % of graphene oxide in water. A similar trend could also be observed for wear track widths shown in Figs. 5.9 (b), 5.10 (b), 5.11 (b), 5.12 (b), and 5.13 (b). The addition of 0.1 wt. % of graphene oxide in water has shown the smallest diameter and wear track width in the present study, as evident from Fig. 5.12 and the reduction in wear scar diameter and wear track width is found to be about 34% and 36%, respectively, when compared with pure water.

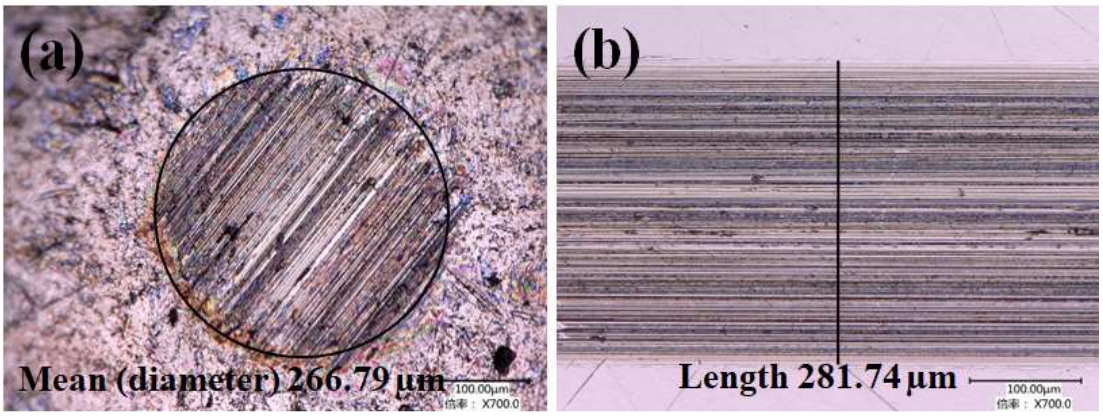

Fig. 5.9 Optical micrographs of wear scar (a) and wear track (b) on the ball and disc, respectively, after the friction test under pure water lubrication at a normal load of 5 N.

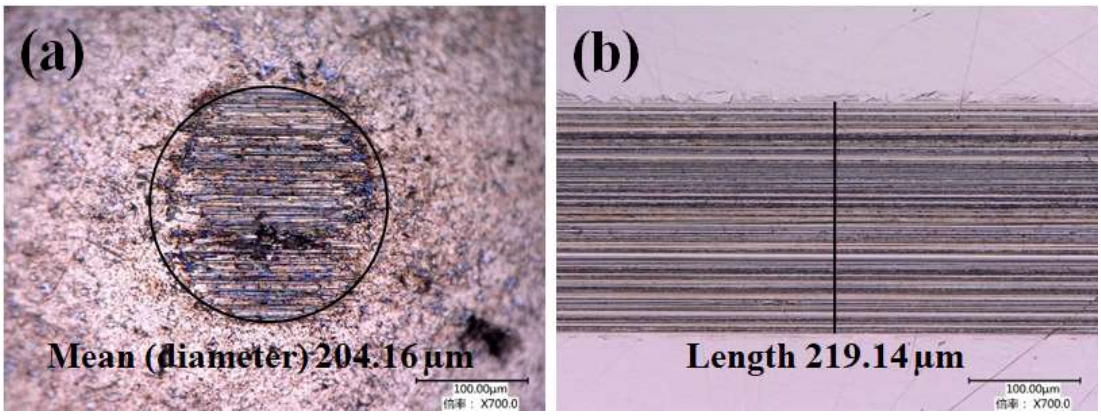

Fig. 5.10 Optical micrographs of wear scar (a) and wear track (b) on the ball and disc, respectively, after the friction test lubricated with 0.01 wt. % graphene oxide in water at a normal load of 5 N.

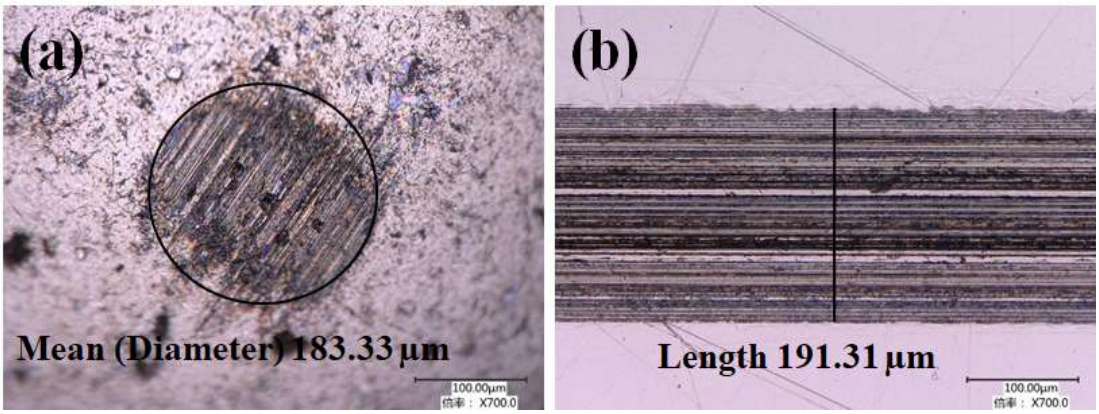

Fig. 5.11 Optical micrographs of wear scar (a) and wear track (b) on the ball and disc, respectively, after the friction test lubricated with 0.05 wt. % graphene oxide in water at a normal load of 5 N.

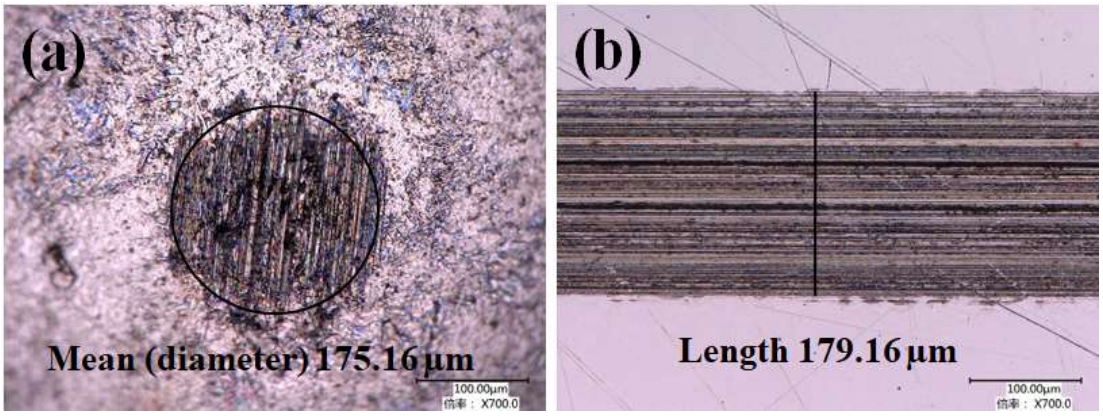

Fig. 5.12 Optical micrographs of wear scar (a) and wear track (b) on the ball and disc, respectively, after the friction test lubricated with 0.1 wt. % graphene oxide in water at a normal load of 5 N.

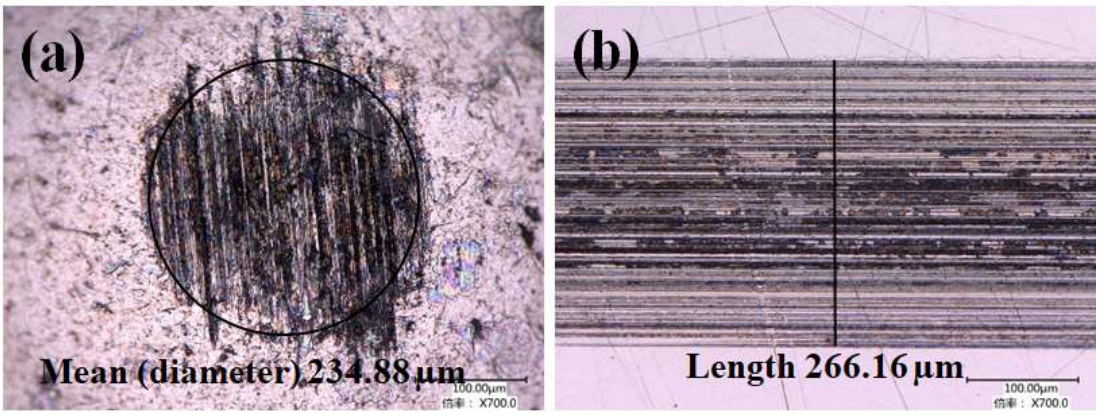

Fig. 5.13 Optical micrographs of wear scar (a) and wear track (b) on the ball and disc, respectively, after the friction test lubricated with 0.5 wt. % graphene oxide in water at a normal load of 5 N.

Figure 5.14 gives the wear volume of steel ball after the friction tests for different concentrations of graphene oxide in water. The estimated wear volume of the steel ball for pure water is approximately 9.98×10^{-5} mm^3. The wear volumes of the ball after the friction tests for different concentrations of graphene oxide in water, i.e., 0.01, 0.05, 0.1, and 0.5 wt. %, as determined by the calculations, are found to be 4.13×10^{-5} mm^3, 3.69×10^{-5} mm^3, 3.16×10^{-5} mm^3, and 7.40×10^{-5} mm^3, respectively. One may observe a significant reduction in wear volume by the addition of just 0.01 wt. % graphene oxide in water, as evident from Fig. 5.14. Among the lubricants containing graphene oxide, the wear volume has been observed to decrease with increasing concentration of graphene oxide from 0.01 to 0.1 wt. %, followed by a slight increase for 0.5 wt.%, the largest amount of additive used in the present work. The wear volume is found to decrease by 68% for 0.1 wt. % graphene oxide concentration, in comparison to that of pure water. The lubricant containing 0.1 wt. % graphene oxide in water has shown the lowest coefficient of friction and the lowest wear volume under the conditions used in the present study, as seen from Figs. 5.7 and 5.14. Hence, it may be concluded that 0.1 wt. % graphene oxide

is the optimum amount in water under the present work. Therefore, further testing at different loads and speeds has been conducted for 0.1 wt. % graphene oxide in water.

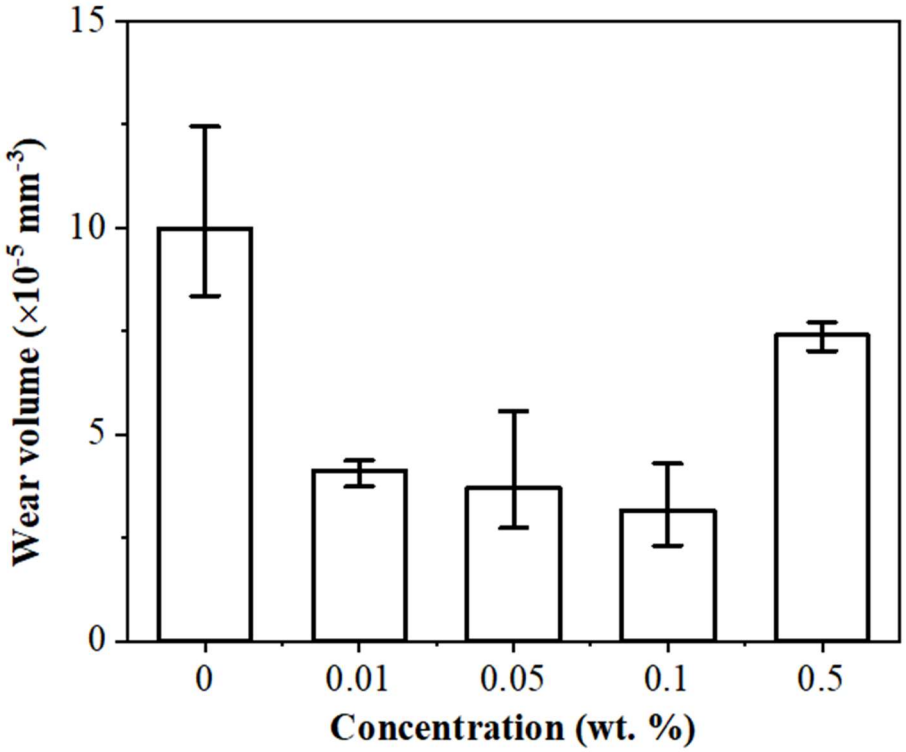

Fig. 5.14 Wear volume of stainless steel balls as a function of the concentration of graphene oxide in water at a normal load of 5 N.

Figures 5.15 to 5.19, show the typical HRSEM micrographs of worn tracks of the disc lubricated with pure water and with different concentrations of graphene oxide (0.01, 0.05, 0.1 and 0.5 wt. %) in water after the friction tests and corresponding energy dispersive spectroscopy (EDS) of the whole surface. It can be noticed that the surface under pure water lubrication, as shown in Fig. 5.15 (a) has wider and deeper tracks and presents a rough surface with some black regions indicating the occurrence of abrasive wear. In contrast, the SEM of worn surface slid under the lubrication of 0.01 wt. % graphene oxide-water dispersion depicts a smoother surface with relatively shallow and

less wide tracks, as evident from Fig. 5.16 (a). The worn surfaces given in Figs. 5.17 (a) and 5.18 (a) corresponding to 0.05 and 0.1 wt. % addition of graphene oxide (GO) present very smooth appearance with only marginal signs of visible tracks (especially in Fig. 5.18 (a)), which are covered with a tribo-layer probably containing graphene oxide. Also, the tribo-layer appears to have covered a larger area of the surface in Fig. 5.18 (a) than in Fig. 5.17 (a), which might have helped in inhibiting the metal-to-metal contact. However, for 0.5 wt. % graphene oxide in water, one may observe a rough surface along with the presence of relatively deeper and wider wear tracks, as evident in Fig. 5.19 (a), which may be due to the abrasive action of agglomerated graphene oxide nano-sheets.

The EDS analysis of the wear tracks after the sliding tests shows the increase in carbon peak intensity and carbon percentage with increasing concentration of graphene oxide in water in the EDS spectrum, as can be seen in Figs. 5.15 (b), 5.16 (b), 5.17 (b), 5.18 (b), and 5.19 (b).

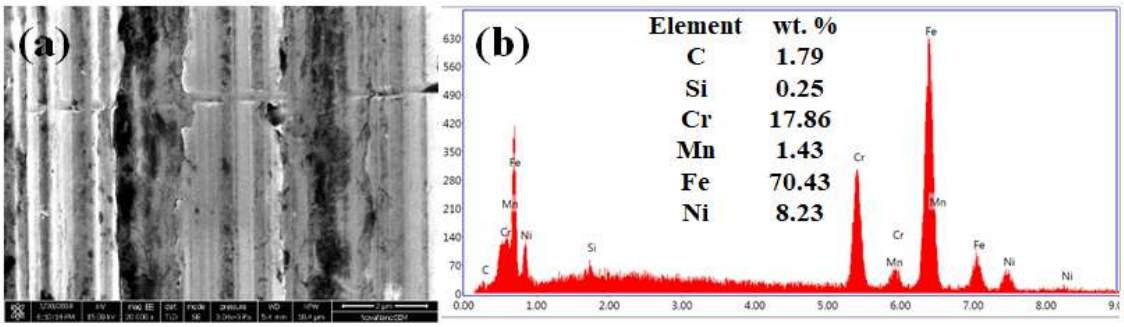

Fig. 5.15 HRSEM micrograph (a) and energy dispersive spectroscopy (EDS) analysis (b) of wear track lubricated with pure water.

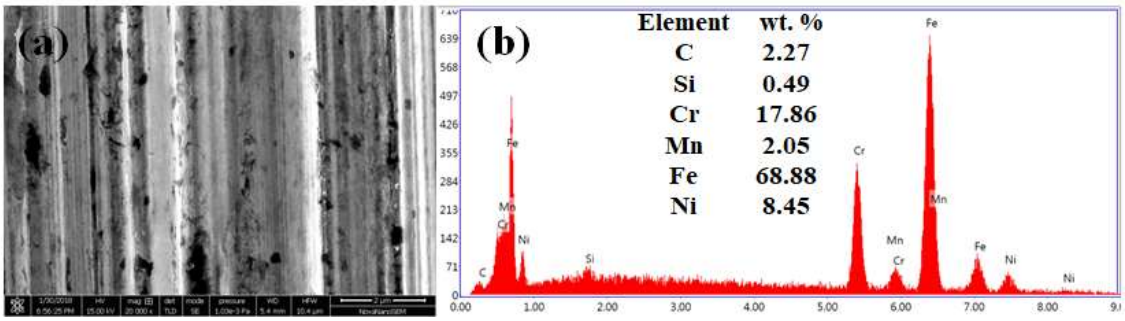

Fig. 5.16 HRSEM micrograph (a) and energy dispersive spectroscopy (EDS) analysis (b) of wear track lubricated with 0.01 wt. % graphene oxide in water.

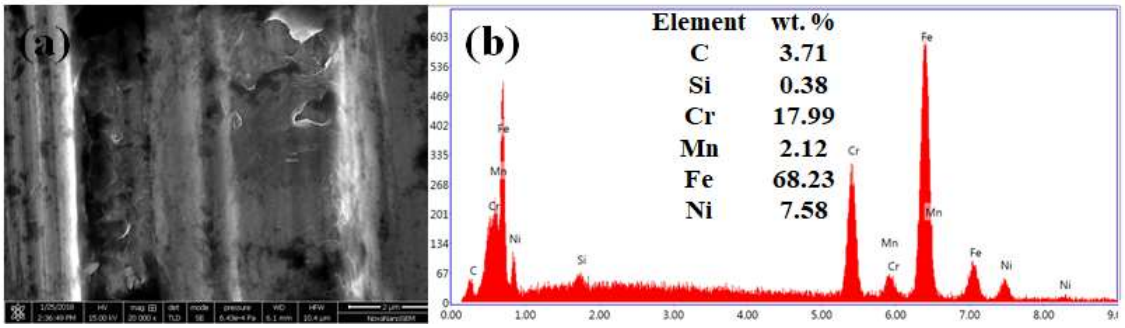

Fig. 5.17 HRSEM micrograph (a) and energy dispersive spectroscopy (EDS) analysis (b) of wear track lubricated with 0.05 wt. % graphene oxide in water.

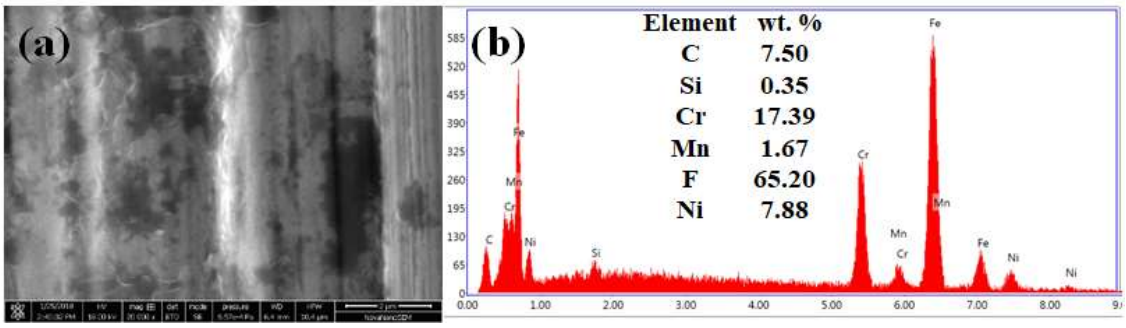

Fig. 5.18 HRSEM micrograph (a) and energy dispersive spectroscopy (EDS) analysis (b) of wear track lubricated with 0.1 wt. % graphene oxide in water.

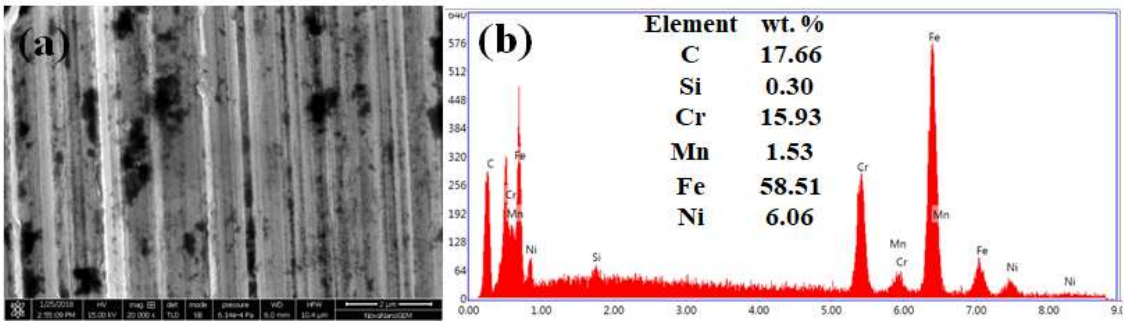

Fig. 5.19 HRSEM micrograph (a) and energy dispersive spectroscopy (EDS) analysis (b) of wear track lubricated with 0.5 wt. % graphene oxide in water.

Further, the worn surfaces have been subjected to Raman spectroscopy to confirm the formation of the graphene tribo-layer on both the contact surfaces and the obtained results have been compared with the Raman spectrum of pristine graphene oxide used in the present study. Figure 5.20 presents the Raman spectra of the worn surfaces of the ball as well as of the disc lubricated with 0.1 wt. % graphene oxide-water dispersion after the sliding test and that of pristine graphene oxide. One may observe the presence of all the three characteristic peaks corresponding to the wear scar and wear track on the ball and disc, respectively, as shown by the pristine graphene oxide, confirming thus, the presence of graphene oxide tribo-layer on the worn surfaces of both the ball and the disc. The patterns of peaks for pristine graphene oxide and the graphene oxide adsorbed on the wear track and wear scar have been found to be similar with only change in I_D/I_G ratio, which is 0.93 for pristine graphene oxide and 1.11 and 1.13, respectively, for graphene oxide on worn surfaces of the ball and the disc, reflecting thus, an increase in D peak intensity on the worn surfaces of the ball and the disc.

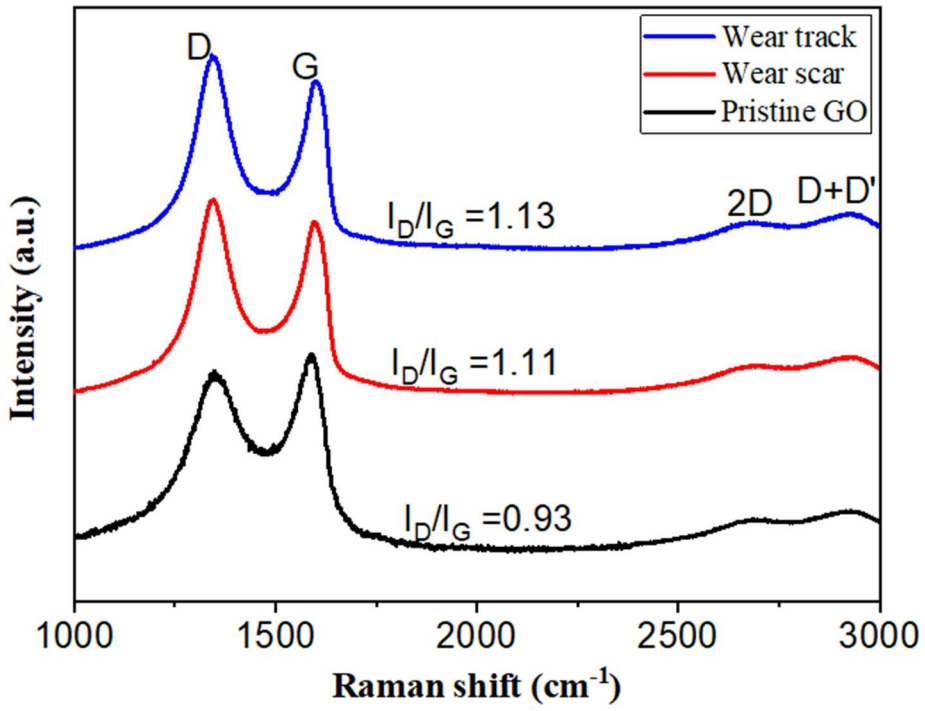

Fig. 5.20 Raman spectra of the pristine graphene oxide and worn surfaces of ball and disc lubricated with 0.1 wt. % graphene oxide in water at a normal load of 5 N.

The formation of the tribo-layer in the contact area has also been confirmed by examining the worn surfaces under TEM. Figure 5.21 (a) presents the schematic area of the wear scar and wear track from where the samples for TEM have been extracted. Figures 5.21 (b and c) show the cross-sectional TEM images of the tribo-film on the steel disc, and it can be seen from Fig. 5.21 (b) that the thickness of the layer formed over the disc surface is about 25 ± 5 nm. Figures 5.21 (d, e, and f) present the cross-sectional TEM images of tribo-film on the steel ball, and it can be observed from Fig. 5.21 (d) that the layer thickness formed over the surface is about 50 ± 10 nm. It is clear from Figs. 5.21 (b and d) that the thickness of the tribo-layer is higher on the ball surface than that on the disc surface. The contact area contains the graphene stacked layers, fragments of graphene oxide sheets, and a matrix of amorphous carbon, as evident from TEM images shown in Figs. 5.21 (c, e, and f). The d-spacing for graphene layers has been found to be

about 0.42 nm, which is larger than that of pristine graphite, which has d (002) value of 0.33 nm.

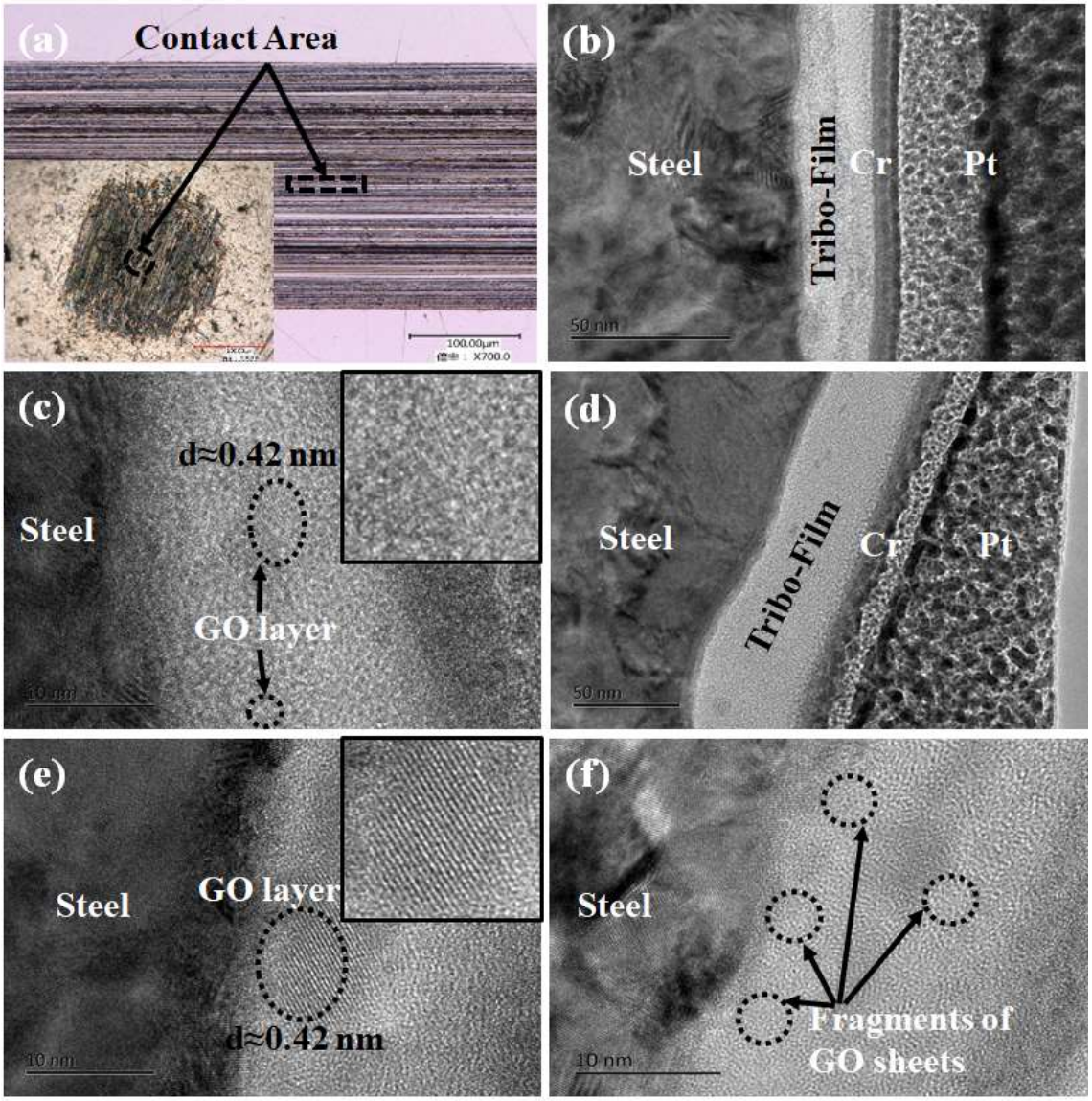

Fig. 5.21 (a) Schematic of the contact area of friction pair, (b, c) cross-sectional TEM image of the tribo-film on the disc, (d, e, f) cross-sectional TEM image of the tribo-film on the ball lubricated with 0.1 wt. % graphene oxide (GO) in water after the friction test at a normal load of 5 N.

5.1.6.2 Effect of Normal Load on Tribological Behaviour

Based on the results presented above, a concentration of 0.1 wt. % graphene oxide in water has been found to be optimum as it has shown the least coefficient of friction and wear volume under the test conditions. Hence, further tests have been conducted at different normal loads of 5, 10, 15 and 20 N to explore the effect of load on the friction and wear behaviour of tribo-pair for the optimised concentration (i.e., 0.1 wt. %) at a speed of 0.01 m/s for 3600 cycles corresponding to a sliding distance of 36 m. The variation of coefficient of friction as a function of the number of cycles is illustrated in Fig. 5.22. Almost the same frictional behaviour can be observed for the normal loads of 5, 10, and 15 N during the initial 700 cycles. After that, the coefficient of friction for 10 and 15 N has been found to increase gradually while the coefficient of friction for 5 N load is comparatively low and steady. For a normal load of 20 N, the coefficient of friction is higher in the beginning, and this behaviour is observed to continue till the completion of the test with a gradual increase in the coefficient of friction with the number of cycles.

For a better understanding of the load-coefficient of friction relation, the variation of the average coefficient of friction with the normal load is presented in Fig. 5.23. The average value of the coefficient of friction has been observed to increase with increasing normal load. The average coefficients of friction at different normal loads of 5, 10, 15, and 20 N, corresponding to contact pressures of 1.42, 1.79, 2.05, and 2.26 GPa have been found to be 0.12, 0.15, 0.16 and 0.19, respectively.

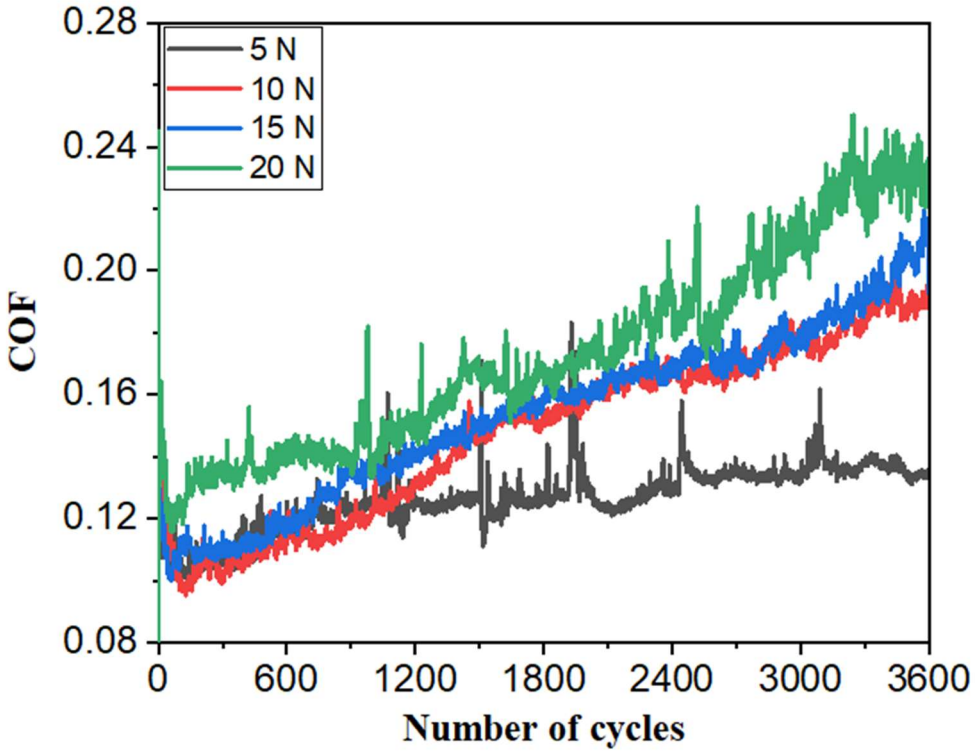

Fig. 5.22 Coefficient of friction as a function of the number of cycles for different normal loads lubricated with 0.1 wt. % graphene oxide in water.

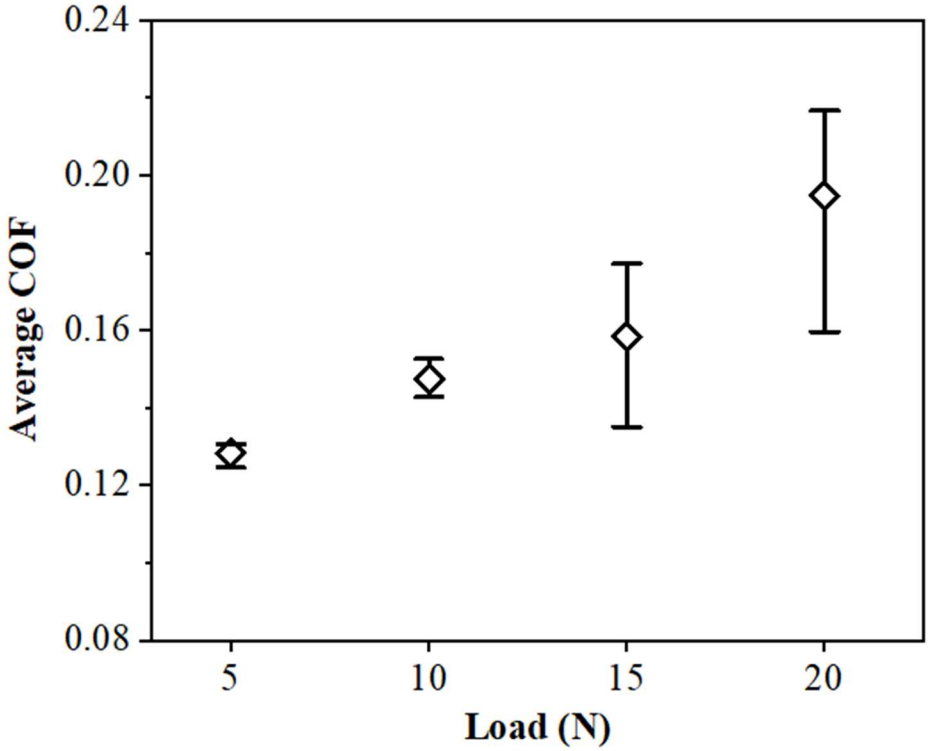

Fig. 5.23 Variation of the average coefficient of friction with different normal loads lubricated with 0.1 wt. % graphene oxide in water.

Figures 5.24 (a to f) illustrate the optical micrographs of wear scar on the ball and the corresponding wear track on the disc slid under 0.1 wt. % of graphene oxide-water dispersion at different normal loads of 10, 15, and 20 N and a sliding speed of 0.01 m/s for 3600 cycles. One could observe an increase in both the wear scar diameter on the ball and the wear track width on the corresponding disc as the load is increased from 5 to 10 N, as evident from a comparison of Figs. 5.12 (a and b) and Figs. 5.24 (a and b). The wear scar diameter and corresponding wear track width at a normal load of 10 N are ~ 265 μm and ~ 293 μm, respectively. Figures 5.24 (c and d) show that the wear scar diameter and wear track width at a normal load of 15 N are ~ 284 μm and ~ 309 μm, respectively. Further, increasing the normal load to 20 N causes an increase in severity of wear, and the values of wear scar diameter and wear track width are found to be ~ 313 μm and ~ 340 μm, respectively, as shown in Figs. 5.24 (e and f). A comparison of wear scars at different normal loads shown in Figs. 5.24 (a, c and e) indicates that wear scar diameter increases with an increase in normal load. A similar trend can be observed for wear track widths shown in Figs. 5.24 (b, d, and f).

The HRSEM micrographs of the tracks of the discs worn under different normal loads of 10, 15, and 20 N are presented in Figs. 5.25, 5.26, and 5.27, respectively. Figure 5.25 shows the morphology of the worn surface of the disc after sliding at a load of 10 N under lubrication of 0.1 wt. % GO-water dispersion. One may observe the presence of a tribo-layer, which appears to be torn at few places along with wider grooves covered with a layer parallel to the direction of sliding. The surfaces worn at the loads of 15 and 20 N and given in Figs. 5.26 and 5.27, respectively, present some relatively wider and deeper grooves parallel to the direction of sliding covered with a fragmented tribo-layer along with some black regions probably of agglomerated GO. The severity of wear

appears to have increased with increasing load from 5 to 20 N, which may be judged from a comparison of Figs. 5.18 (a), 5.25, 5.26, and 5.27.

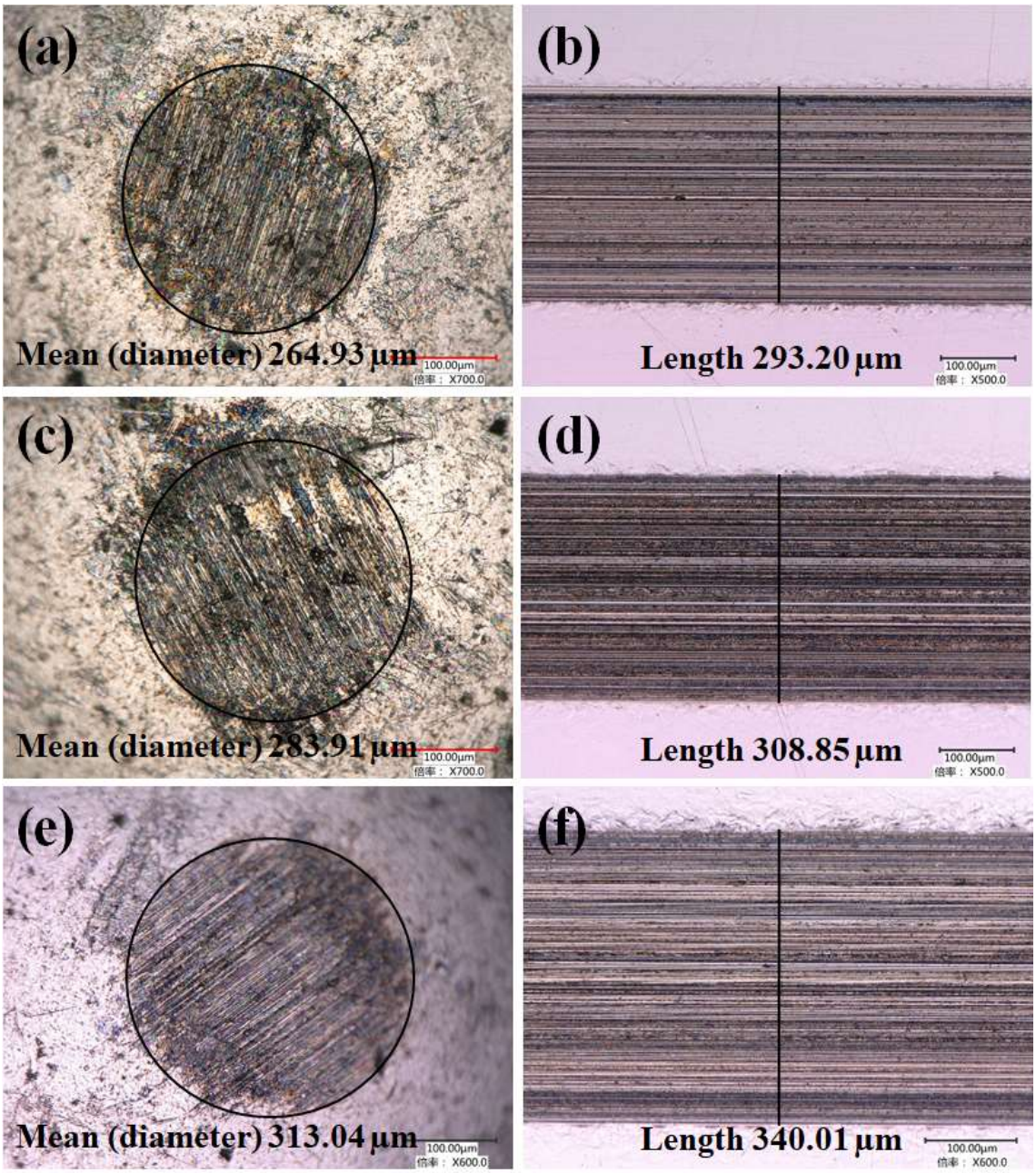

Fig. 5.24 Optical micrographs of wear scars (a, c, e) and corresponding wear tracks (b, d, f) on the ball and disc, respectively, lubricated with 0.1 wt. % graphene oxide in water under the normal load of 5 N (a, b), 10 N (c, d), and 20 N (e, f).

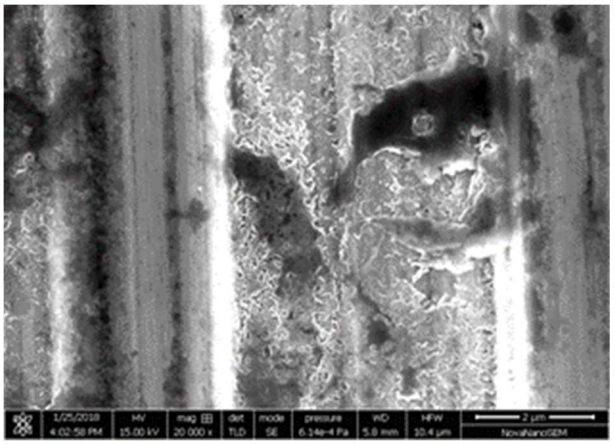

Fig. 5.25 HRSEM micrographs of wear track lubricated with 0.1 wt. % graphene oxide in water at a normal load of 10 N.

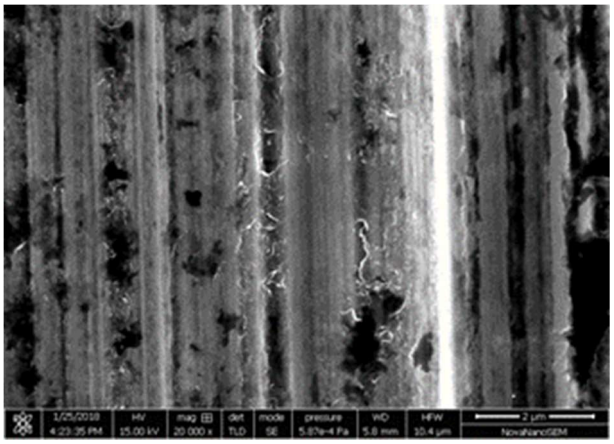

Fig. 5.26 HRSEM micrographs of wear track lubricated with 0.1 wt. % graphene oxide in water at a normal load of 15 N.

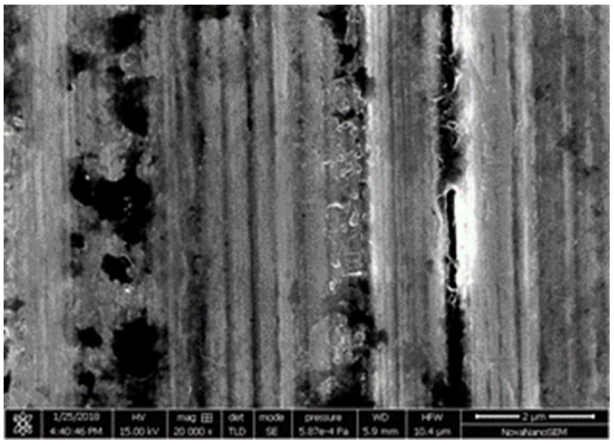

Fig. 5.27 HRSEM micrographs of wear track lubricated with 0.1 wt. % graphene oxide in water at a normal load of 20 N.

Figure 5.28 presents the relationship between the wear volume and normal load, and wear volume has been observed to increase linearly with the load. The wear volumes of the ball after the friction tests at different normal loads, i.e., 5, 10, 15, and 20 N for 0.1 wt. % graphene oxide in water have been calculated to be 3.16×10^{-5} mm^3, 12.31×10^{-5} mm^3, 16.32×10^{-5} mm^3, and 23.38×10^{-5} mm^3, respectively. As evident from Fig. 5.28, the wear volume of the ball at a normal load of 5 N is about 83.4% less compared to that at 20 N.

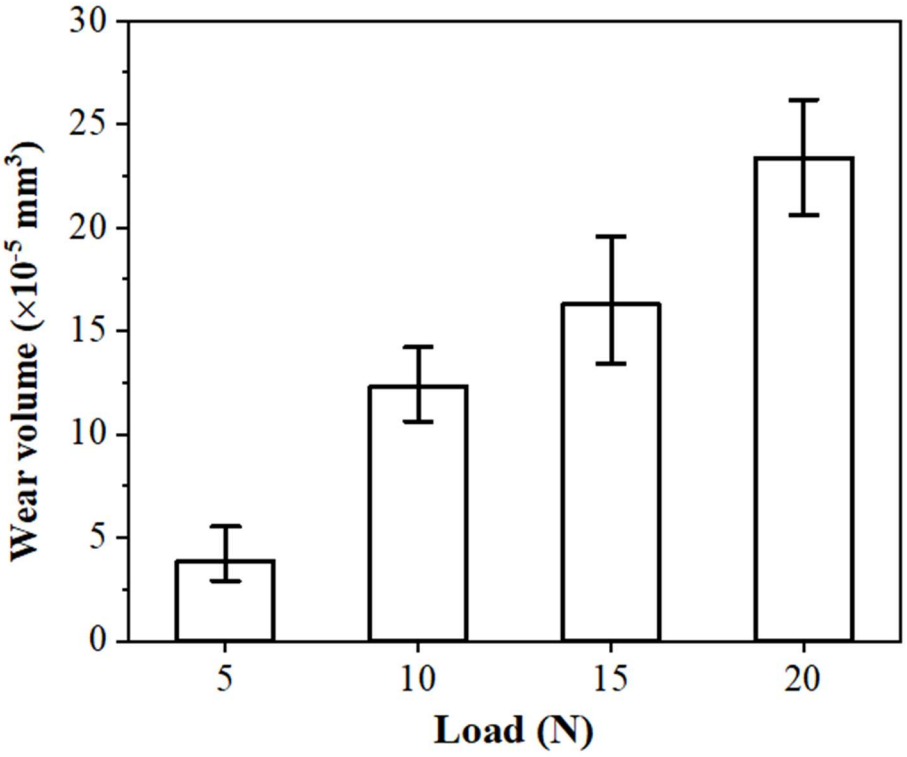

Fig. 5.28 Wear volume of counter-face steel ball as a function of normal load for 0.1 wt. % graphene oxide in water.

5.1.6.3 Effect of Sliding Speed on Tribological Behaviour

On the basis of the results on friction and wear performance of tribo-pair presented above for different loads and concentrations of graphene oxide in water, a normal load of 5 N and a concentration of 0.1 wt. % graphene oxide in water have been found to be optimum. Hence, further tests have been conducted for different sliding speeds to investigate the effect of sliding speed on the friction and wear behaviour of tribo-pair for optimised load (i.e., 5 N) and concentration of GO in water (i.e., 0.1 wt. %) for a duration of 3600 cycles corresponding to a sliding distance of 36 m. The ball has been slid against the stationary disc under different sliding speeds of 0.005, 0.01, 0.05, and 0.1 m/s, corresponding to 0.5, 1, 5, and 10 Hz reciprocating frequency over a stroke length of 5 mm. Figure 5.29 shows a fluctuating trend of variation of coefficient of friction with the number of cycles at a Hertzian contact pressure of 1.42 GPa (normal load of 5 N). However, the amplitude of fluctuations is observed to decrease with increasing speed.

Figure 5.30 depicts the variation of the average coefficient of friction (COF) with sliding speed. One may observe that the average coefficient of friction decreases with an increase in speed from 0.005 to 0.05 m/s, beyond which it increases for 0.1 m/s, indicating that a speed of 0.05 m/s is the optimum speed. The average coefficients of friction for different sliding speeds i.e., 0.005, 0.01, 0.05, and 0.1 m/s are 0.17, 0.12, 0.11, and 0.16, respectively.

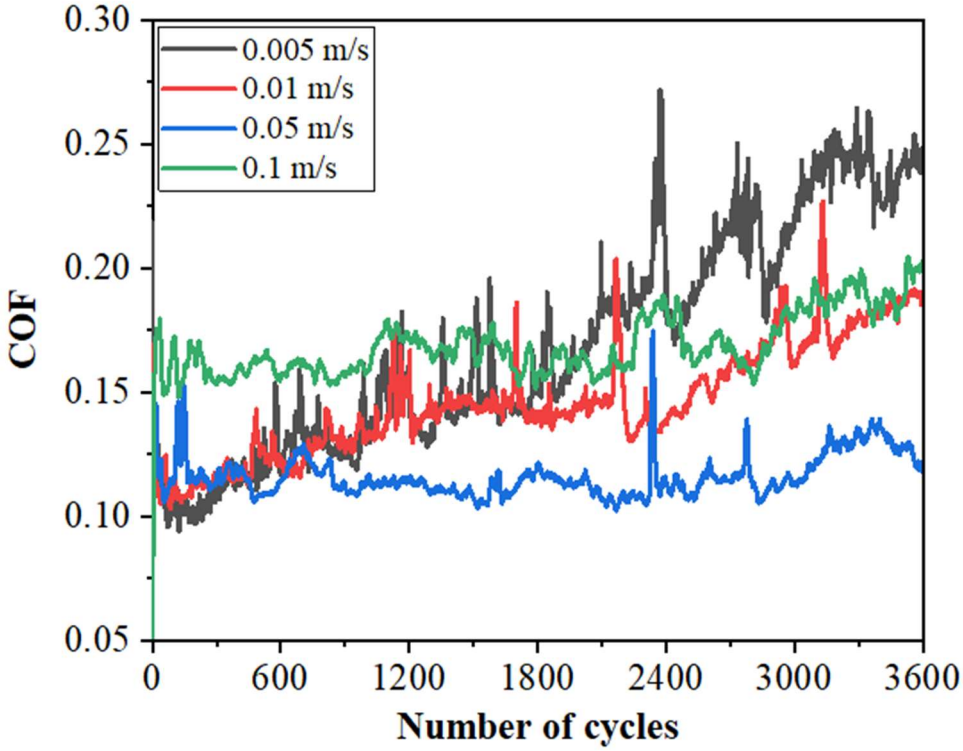

Fig. 5.29 Coefficient of friction as a function of cycles for different sliding speeds for 0.1 wt. % graphene oxide in water at a normal load of 5 N.

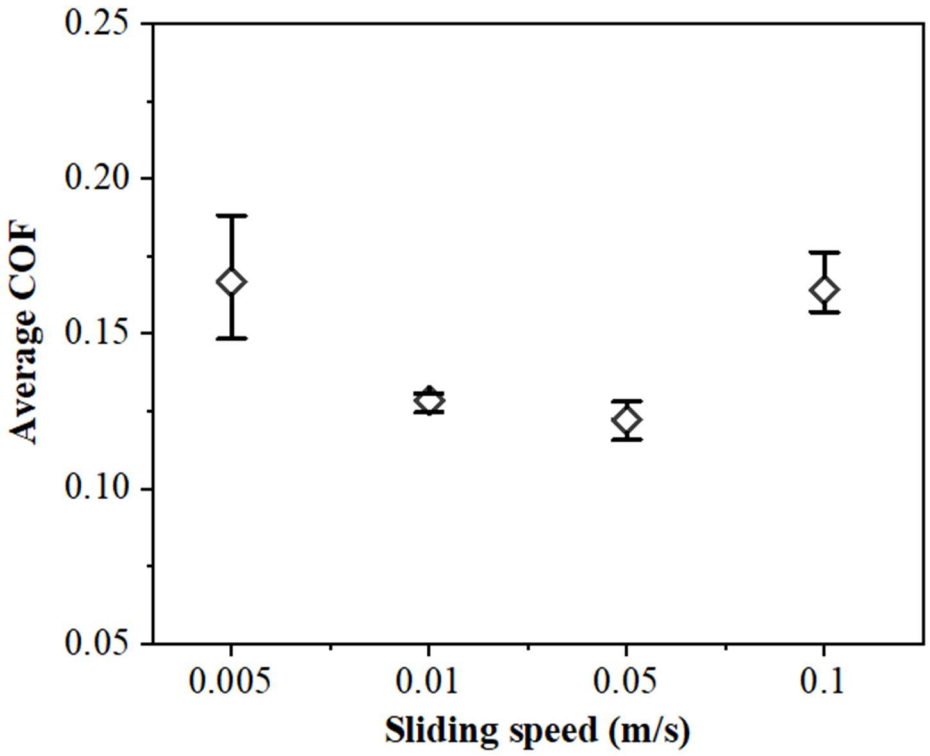

Fig. 5.30 Variation of the average coefficient of friction with sliding speed lubricated with 0.1 wt. % graphene oxide in water at a normal load of 5 N.

Figures 5.31 (a to f) presents the optical micrographs showing wear scar diameter on the balls and corresponding wear track width on discs after the sliding test at a normal load of 5 N for different sliding speeds of 0.005, 0.05, and 0.1 m/s for 3600 cycles. It can be observed in Figs. 5.31 (a and b) that wear scar diameter and wear track width for sliding speed of 0.005 m/s are about ~ 226 μm and ~ 261 μm, respectively. Increasing speed to 0.01 m/s causes a reduction in wear scar diameter and wear track width to ~ 175 μm and ~ 179 μm, respectively (Fig. 5.12 (a and b)). Wear scar diameter and wear track width have been found to be ~ 169 μm and ~ 173 μm, respectively, for a sliding speed of 0.05 m/s, as evident from Fig. 5.31 (c and d), which are slightly smaller than those found for 0.01 m/s. Both the wear scar and wear track width have been observed to increase to ~ 217 μm and ~ 232 μm at a speed of 0.1 m/s as mentioned in Fig. 5.31 (e and f). From the above-reported results, it can be concluded that the sliding speed of 0.05 m/s has the minimum wear scar diameter and wear track width among all the speeds used in the current study.

The HRSEM micrographs of the surfaces worn under 0.1 wt. % graphene oxide-water dispersion at a normal load of 5 N and sliding speeds of 0.005, 0.05, and 0.1 m/s have been illustrated in Figs. 5.32 to 5.34. The worn surface corresponding to a speed of 0.005 m/s (Fig. 5.32) reveals relatively deeper and wider grooves parallel to the direction of sliding indicating a severely damaged and rough surface. One may observe a smooth surface (Fig. 5.33) with very shallow grooves in the direction of sliding corresponding to a sliding speed of 0.05 m/s. However, increasing the speed to 0.1 m/s (Fig. 5.34) leads to a relatively rougher surface with increased depth and width of grooves, which might have raised the friction for this speed in comparison to 0.05 m/s.

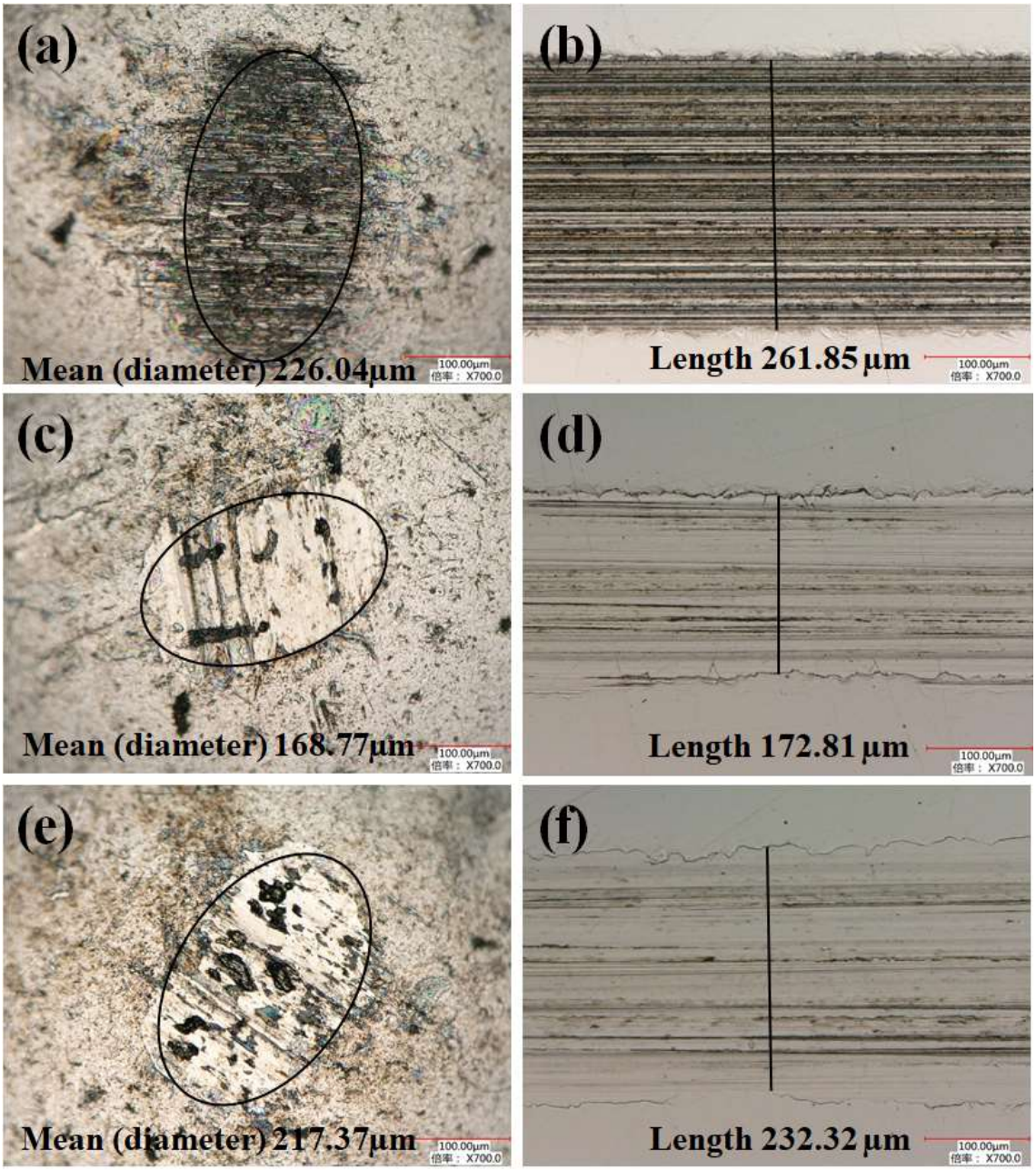

Fig. 5.31 Optical micrographs of wear scars (a, c, e) on the ball and corresponding wear tracks (b, d, f) on the disc, respectively, for a sliding speed of 0.005 m/s (a, b), 0.05 m/s (c, d), and 0.1 m/s (e, f) lubricated with 0.1 wt. % graphene oxide in water at a normal load of 5 N.

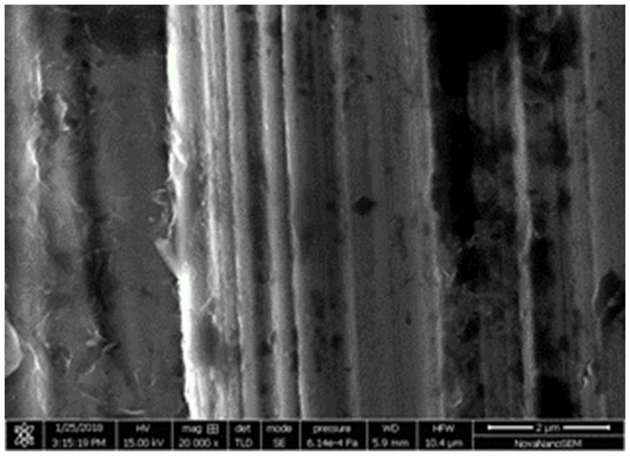

Fig. 5.32 HRSEM micrographs of wear track lubricated with 0.1 wt. % graphene oxide in water at a normal load of 5 N for a sliding speed of 0.005 m/s.

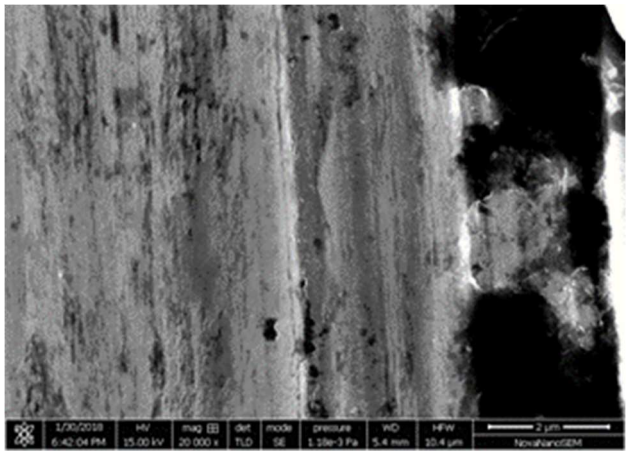

Fig. 5.33 HRSEM micrographs of wear track lubricated with 0.1 wt. % graphene oxide in water at a normal load of 5 N for a sliding speed of 0.05 m/s.

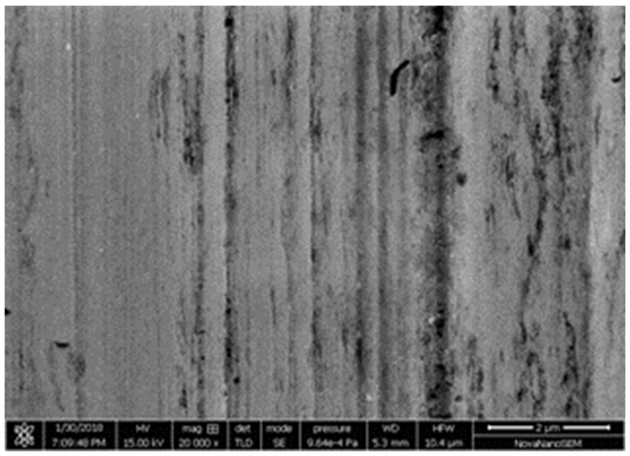

Fig. 5.34 HRSEM micrographs of wear track lubricated with 0.1 wt. % graphene oxide in water at a normal load of 5 N for a sliding speed of 0.1 m/s.

Figure 5.35 provides the variation of wear volume of the ball as a function of sliding speed after the friction tests at a normal load of 5 N under 0.1 wt. % graphene oxide-water dispersion. It can be observed that the ball wear volume decreases with increasing sliding speed from 0.005 m/s to 0.05 m/s, followed by an increase for 0.1 m/s. The calculated wear volumes of the ball after the friction test for different sliding speeds of 0.005, 0.01, 0.05, and 0.1 m/s for 0.1 wt. % graphene oxide in water are found to be 6.11×10^{-5} mm^3, 3.16×10^{-5} mm^3, 3.02×10^{-5} mm^3, and 5.44×10^{-5} mm^3, respectively. The minimum wear volume has been found to occur for a sliding speed of 0.05 m/s. Hence, it may be concluded that 0.05 m/s is the optimum speed at a normal load of 5 N under the lubrication of 0.1 wt. % graphene oxide in water.

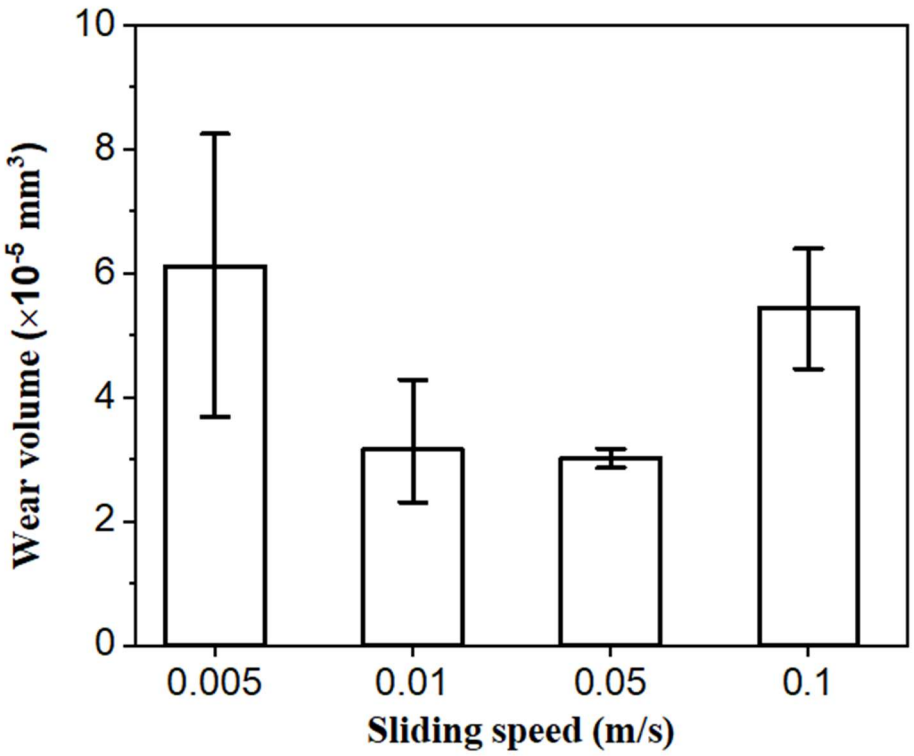

Fig. 5.35 Wear volume of the counter-face steel ball as a function of sliding speed lubricated with 0.1 wt. % graphene oxide in water at a normal load of 5 N.

5.2 DISCUSSION

Raman spectroscopy is one of the best tools to characterise the graphene and related materials, hence the graphene oxide powder has been initially characterised by Raman spectroscopy. The presence of three main characteristic peaks (D, G, and 2D) shown in Fig. 5.2 for graphene oxide is in consonance with the observations reported earlier by Stankovich et al., (2007) and Childres et al., (2013). Strong D and G peaks observed in Fig. 5.2 indicate a very small size of the crystal, which has further been supported by AFM and TEM. 2D AFM image (Fig. 5.4) and TEM image (Fig. 5.5) confirm that the thickness of dispersed graphene oxide nano-sheets is about ~ 1.2 nm with the size not more than 5 μm. A higher thickness observed at the centre of the AFM image might be due to the overlapping of two layers, as evident from Fig. 5.4. The layered structure of graphene oxide is evident from the TEM image given in the inset in Fig. 5.5. The increase in viscosity with increasing graphene oxide concentration in water, as seen in Fig. 5.6, may be attributed to the increased probability of agglomeration of graphene oxide nano-sheets with the increasing amount of graphene oxide. A similar trend of viscosity variation has also been reported earlier by Azman et al. (2016).

The friction and wear behaviour are known to be sensitive to the lubricants, working conditions (i.e., load, sliding speed, environment, temperature), and the properties of the mating materials in sliding contact. To enhance the lubricating potential of existing lubricants, additives are added, and the concentration of additives in a lubricant plays a vital role in improving the tribological performance. Too high or too low concentrations may deteriorate the anti-friction and anti-wear performance of an additive in the lubricant. The variation of coefficient of friction with the number of cycles presented in Fig. 5.7 shows that the pure water has large fluctuations and a high

coefficient of friction throughout the friction test. This may be ascribed to a relatively lower viscosity (Fig. 5.6) and low pressure-viscosity coefficient of water. A significant decrease in coefficient of friction with the addition of graphene oxide nano-sheets in water, as evident from Fig. 5.7, may be attributed to the adsorbtion of graphene oxide nano-sheets on the surfaces of mating bodies which provide low shearing properties at the interface.

The average coefficient of friction decreases with an increasing amount of graphene oxide from 0.01 to 0.1 wt. %, which is followed by a slight increase for 0.5 wt. % (Fig. 5.8), indicating that 0.1 wt. % is the optimum content of graphene oxide under the conditions used in the present investigation. The lower and the higher concentrations of graphene oxide have shown relatively higher coefficients of friction in comparison to 0.1 wt. %, as evident from Fig. 5.8, which may be attributed to the deterioration in the lubricating performance either due to inadequate or excess amounts of graphene oxide in water depending on the amount of addition of graphene oxide.

A relatively higher coefficient of friction observed for pure water lubrication (Fig. 5.8), may be explained on the basis of the SEM micrograph of the worn surface of disc given in Fig. 5.15 (a), which presents a rough surface with wider and deeper grooves indicating the occurrence of abrasive wear due to direct asperity-asperity contact between the ball and disc. A significant decrease in coefficient of friction with the addition of graphene oxide in water, as seen from Fig. 5.8, may be attributed to the formation of a tribo-layer probably of graphene oxide (GO) nano-sheets adsorbed on the disc as seen from Fig. 5.16 (a). This layer hinders the metal-to-metal contact and provides low shearing capability at the interface, both of which result in reduced friction. The extent of formed tribo-layer is purely dependent on the amount of graphene oxide added in water,

as observed for Figs. 5.16 (a), 5.17 (a), 5.18 (a), 5.19 (a). For the concentration lower than 0.1 wt. %, the adequate amount of graphene oxide nano-sheets is not available for the formation of a continuous layer over the friction surfaces as depicted in Figs. 5.16 (a), 5.17 (a), which results in partial metal-to-metal contact. However, a highly smooth tribo-layer is formed on the disc surface for a graphene oxide concentration of 0.1 wt. %, as evident in Fig. 5.18 (a). An increasing concentration of GO in water facilitates the formation of tribo-layer, which is able to cover a relatively larger area of the surface and may be judged from a comparison of Figs. 5.16 (a), 5.17 (a) and 5.18 (a) corresponding to 0.01, 0.05 and 0.1 wt. % addition of GO. The larger extent of cover provided by the tribo-layer to the underlying material offers more hindrance to the direct metal-to-metal contact and leads to a reduction in friction. The presence of tribo-layer of adsorbed GO nano-sheets on the surface of both the ball and the disc has been confirmed by Raman spectra given in Fig. 5.20 and the TEM of the worn surfaces of the disc and the ball depicted in Figs. 5.21 (b, c) and 5.21 (d ,e, f), respectively. The presence of D, G and 2D peaks and similar trends of Raman spectrum of pristine graphene oxide powder, wear scar and wear track confirm that there is a layer of graphene oxide on the surface of both the ball and the disc after the sliding test. An increase in D peak intensity in the Raman spectrum of the worn surface of the ball, as well as of the disc in Fig. 5.20, could also be seen, which points toward an increase in the defect and disordering of graphene oxide during the sliding process due to the presence of high contact pressure on graphene oxide nano-sheets (Zheng et al., 2016). Thus, the Raman spectrum of ball and disc confirms the presence of the graphene layer on the rubbing surfaces with slightly increased defects concentration. The tribo-layer on both surfaces has also been confirmed by TEM, as shown in Fig. 5.21. Tribo-layer can be observed clearly over the surfaces after the sliding tests. A higher thickness of the tribo-layer on the ball surface can be seen compared to

the disc surface. This higher thickness is attributed to the reason that the ball surface is always in contact while the disc surface comes in contact periodically. The increase in the interlayer spacing may be probably due to the introduction of oxygen functional groups between the graphene layers.

An increase in the coefficient of friction with the addition of 0.5 wt. % GO in water may be attributed to the agglomeration of GO nano-sheets and failure to form a well-spread tribo-layer on the sliding interface, as seen from Fig. 5.19 (a). The agglomerated GO nano-sheets might have also resulted in abrasive action due to increased graphene oxide nano-particles, which could be judged from the presence of some grooves in Fig. 5.19 (a). The increase in carbon peak in EDS with increasing concentration of graphene oxide in water has also been observed in Figs. 5.16 (b), 5.17 (b), 5.18 (b), 5.19 (b), which reflects the increased amount of carbon. The increase in carbon might have occurred due to the adsorbtion of graphene oxide nano-sheets on the surface during the sliding process, which has been confirmed by Raman spectroscopy and TEM examination, as shown in Figs. 5.20 and 5.21.

The addition of 0.01 wt. % graphene oxide in water results in a significant reduction in the wear volume loss in comparison to that for pure water, as seen from Fig. 14, which reflects the effectiveness of graphene oxide addition in improving the anti-wear performance of the lubricant. However, the observed behaviour may also be explained on the basis of the features revealed by the HRSEM micrographs given in Figs. 5.15 (a) and 5.16 (a), corresponding to the surfaces worn under pure water and 0.01 wt. % GO-water dispersion. The presence of relatively deeper and broader grooves in Fig. 5.15 (a) indicates the occurrence of the direct asperity contact between the tribo-pair, which might have resulted in an increased wear, whereas the surface worn under 0.01 wt. % GO-water

dispersion (Fig. 5.16 (a)) presents a relatively smooth surface with the formation of a tribo-layer, which reduces friction and wear by inhibiting direct metal-to-metal contact, as explained above. A decrease in wear volume loss with an increasing amount of GO from 0.01 wt. % to 0.1 wt. % and a slight increase for 0.5 wt. % may also be explained on the basis of (i) the formation of a tribo-layer of graphene oxide nano-sheets on the surfaces of both the ball and the disc, (ii) the extent of cover provided by this layer to the underlying substrate and (iii) the effectiveness of this layer in hindering the direct metal-to-metal contact as explained earlier for friction. One may observe the presence of a smooth tribo-layer on the surface of steel worn under 0.1 wt. % GO-water dispersion (Fig. 5.18 (a)), whereas the worn surfaces under 0.5 wt. % GO-water dispersion (Fig. 5.19 (a)), illustrates a relatively rough surface with grooves running parallel to sliding direction along with the presence of some aggregates of graphene oxide at few locations, indicating the occurrence of abrasion and direct metal-to-metal contact. This may explain a slightly higher friction and wear volume loss observed for relatively larger (> 0.1 wt. %) addition of graphene oxide in water as observed in Figs. 5.8 and 5.14. The agglomeration due to a higher concentration of graphene/graphene-based nano-particles has been reported to result in abrasion (even though these particles are soft), which may have resulted in an increase in both friction and wear, as reported earlier by Liang et al. (2016) and Elomaa et al. (2015). The degradation in anti-wear performance for 0.5 wt. % graphene oxide in water may also be ascribed to the agglomeration of graphene nano-sheets, which results in the formation of lumps and diminishes the chances of formation of a continuous tribo-layer at the sliding interface. Similar observations have also been reported by Guo et al. (2016).

A fluctuating trend of variation of coefficient of friction with the number of cycles at different loads of 5, 10, 15, and 20 N shown in Fig. 5.22 may be due to the formation-scrape-reformation of the tribo-layer, which give rise to intermittent contact between tribo-pair and attainment of better surface compatibility. One may observe that the amplitude of fluctuations is relatively large for the highest load (20 N) in comparison to 5, 10 and 15 N used in the present work. However, the variation of the coefficient of friction is found to be stable at the lowest load of 5 N, whereas the same is observed to increase with increasing the number of cycles and the load. It may be explained on the basis of the presence of a smooth tribo-layer of adsorbed graphene oxide nano-sheets on the disc surface, which provides a low shearing interface and protects the underlying material from being penetrated by the asperities of counterface as seen from HRSEM micrograph of worn surface of disc given in Fig. 5.18 (a). Since the protection provided by the formed tribo-layer is limited by its load-carrying capability, the damage to tribo-layer occurs with increasing load, as evident from HRSEM micrographs given in Figs. 5.25, 5.26, and 5.27 corresponding to surfaces worn under 10, 15 and 20 N, respectively. With an increase in load, the asperities are able to penetrate through the tribo-layer giving rise to metal-to-metal contact and resulting thereby, in an increase in average coefficient of friction as well as wear volume, as evident from Figs. 5.23 and 5.28. The formed tribo-layer gets either fragmented or easily penetrated with the increasing load, which can be judged from a comparison of Figs. 5.18 (a), 5.25, 5.26 and 5.27, which depict the HRSEM micrographs of the surface of disc worn under 5, 10, 15, and 20 N. The increased possibility of fragmentation of layer and penetration of asperities leads to direct metal-to-metal contact and hence, an increase in loss of material as reflected from a relatively larger wear scar diameters and wear track widths shown in Fig. 5.24 and the variation of wear volume with load given in Fig. 5.28. Therefore, on the basis of discussion of results

presented above, one may infer that the addition of 0.1 wt. % graphene oxide in water is effective in improving the friction and wear performance under relatively lower loads compared to higher loads.

The following discussion pertains to the observed friction and wear behaviour of the tribo-pair slid under 0.1 wt. % GO-water lubrication at a fixed load of 5 N and different sliding speeds of 0.005, 0.01, 0.05, and 0.1 m/s. The coefficient of friction decreases with an increase in sliding speed up to 0.05 m/s and increases beyond for a sliding speed of 0.1 m/s over a stroke length of 5 mm, as seen from Fig. 5.30, indicating that 0.05 m/s is the optimum speed for 0.1 wt. % graphene oxide in water under the condition used in the present investigation. A decreasing friction with increasing speed up to 0.05 m/s, as seen from Fig. 5.30, may be attributed to the greater tendency of entrainment of graphene oxide between the contact pairs due to better circulation of graphene oxide sheets between the rubbing surfaces. On the other hand, increasing speed may cause a reduction in time during which asperities remain in contact and resulting in less deformation of asperities and a consequent decrease in the real contact area, which causes a decrease in the coefficient of friction as well as wear seen from Figs. 5.30 and 5.35. A relatively higher coefficient of friction observed for a sliding speed of 0.005 m/s (Fig. 5.30) may be explained on the basis of the HRSEM micrograph of the worn surface given in Fig. 5.32, which presents a damaged and rough surface with relatively deeper and broader grooves parallel to sliding direction pointing toward abrasion by the contacting asperities. As the sliding speed increases to 0.05 m/s, the surface appears to be covered by smooth transfer layer of adsorbed graphene (Fig. 5.33), which might have resulted in relatively less metal-to-metal contact and hence, lower friction and wear. However, for the highest sliding speed of 0.1 m/s used in the present study, the graphene oxide appears to have been moved out of the interface because of relatively high speed

resulting in discontinuous lubrication due to inadequate supply of lubricant. The absence of graphene oxide on the surface has been confirmed by the HRSEM micrograph shown in Fig. 5.34. This might have given rise to metal-to-metal contact and resulted in an increase in both the coefficient of friction and wear at the highest speed of 0.1 m/s used in the present work, as evident from Figs. 5.30 and 5.35.

Based on the results and discussion presented above, the anti-wear and anti-friction mechanism of graphene oxide as lubricant additives can be proposed. Under pure water lubrication, the ball slides over the disc causing abrasive wear mainly. However, the addition of graphene oxide in water brings about a significant decrease in both friction and wear due to the adsorbtion of graphene oxide on contacting surfaces and subsequent formation of a protective tribo-film. This film plays a crucial role in reducing both the friction and the wear by protecting the underlying metal from direct metal-to-metal contact and providing an easy to shear interface between the contacting tribo-pair. However, the tribological performance is found to be dependent on the amount of graphene oxide nano-sheets in the lubricant. At relatively low concentrations (< 0.1 wt. %), adequate nano-sheets are not available to form a continuous tribo-film over the surface whereas, for the higher concentration (> 0.1 wt. %), agglomeration of graphene oxide nano-sheets hampers the formation of tribo-layer. Both of these conditions result in increased friction and wear due to the increased possibility of direct contact between the mating bodies. An increase in friction with the increasing load has been attributed to the increasing penetration of the tribo-layer by the asperities due to increased contact pressure, which results in the loss of effectiveness of this tribo-layer in reducing the friction. For sliding speed up to 0.05 m/s, the tribological properties get improved due to entrainment of graphene oxide nano-sheets between the rubbing surfaces due to better circulation of lubricant between the mating surfaces. However, for a relatively higher

speed of 0.1 m/s, lubricant containing graphene oxide squeezes out of the contact surface due to high speed resulting in discontinuous lubrication and inadequate supply of lubricant between the rubbing surfaces. Since the lubrication can only be provided by the entrapped graphene nano-sheets between the surfaces, the intermittent supply of lubricant leads to an increase in friction and wear at the highest speed of 0.1 m/s. Hence, it may be concluded that the optimum conditions of load, speed and amount of graphene oxide are required to realise its effectiveness in improving the tribological performance of the water-based lubricant.